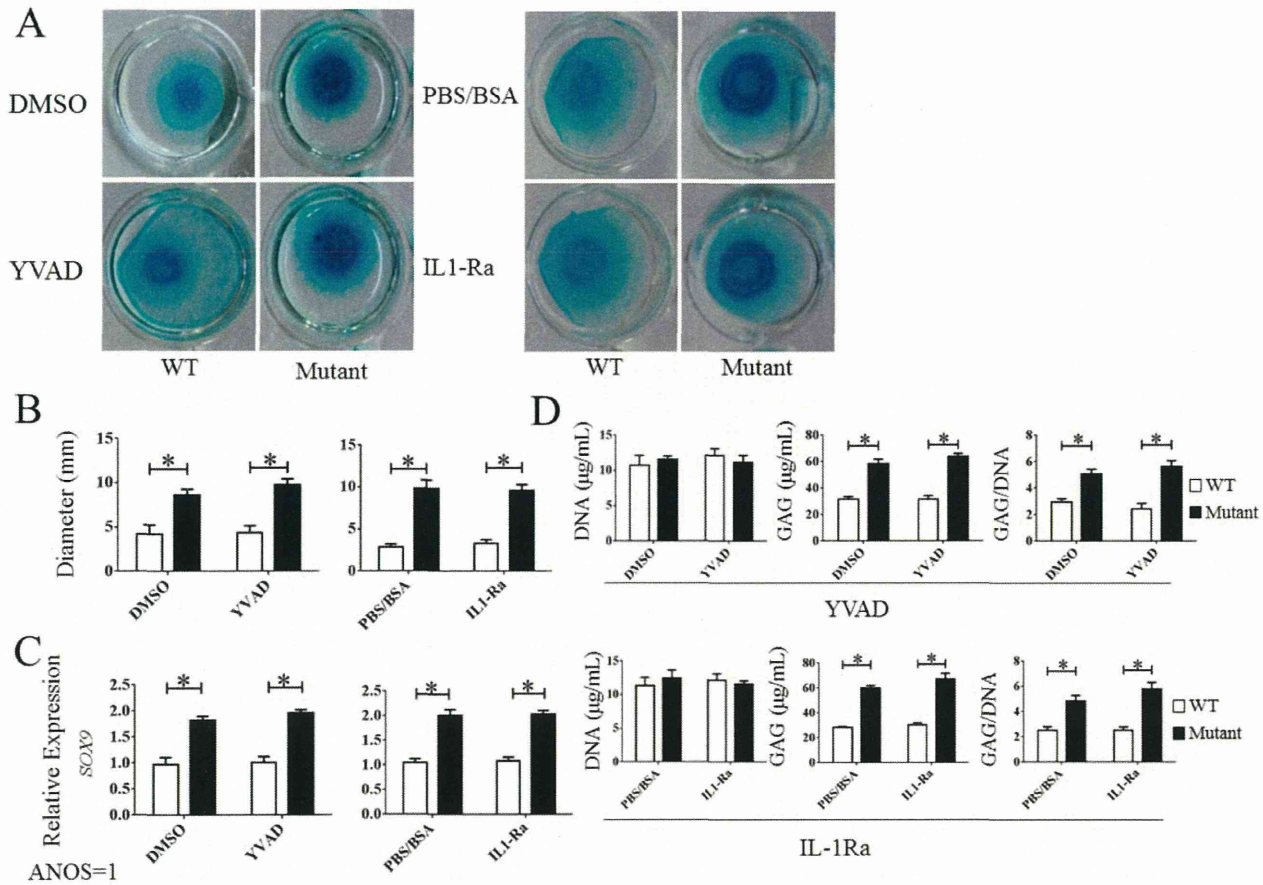

Figure 4. NLRP3 inflammasome–independent enhanced chondrogenesis of mutant iPSCs from patients with neonatal-onset multisystem inflammatory disease. Wild-type and mutant iPSCs were differentiated into chondrocytes in 2-D micromass cultures, and the caspase 1 inhibitor Ac-YVAD-CHO (YVAD; 10 μM) or human recombinant interleukin-1 receptor antagonist (IL-1Ra; 1 μg/ml) was added to the cultures. Control cultures were incubated with DMSO or phosphate buffered saline (PBS) containing bovine serum albumin (BSA). **A**, Representative 2-D micromass cultures treated with YVAD or DMSO as control (left) or with IL-1Ra or PBS/BSA as control (right). **B**, Diameter of the micromass. **C**, *SOX9* expression in chondrocytes derived from wild-type and mutant iPSCs and treated with YVAD or IL-1Ra. Expression levels are shown relative to those in ANOS cells (set at 1). **D**, DNA concentration, glycosaminoglycan (GAG) concentration, and the ratio of GAG concentration to DNA concentration in chondrocytes derived from wild-type or mutant iPSCs and treated with YVAD or IL-1Ra. Bars show the mean ± SEM of 3 independent clones from which triplicate measurements were obtained. Data are representative of 3 independent experiments. Data shown were obtained using iPSCs from patient 1; similar results were obtained using iPSCs from patient 2. * = $P < 0.05$. See Figure 1 for other definitions.

expression of the NLRP3 inflammasome components in 2-D cartilage samples. Mutant and wild-type cartilage samples both expressed NLRP3, but did not express ASC, pro–caspase 1, or pro–IL-1β by Western blotting (data not shown). This suggests that the formation of large cartilaginous masses by mutant chondrocytes occurs independently of the NLRP3 inflammasome.

To confirm that chondrogenesis of mutant iPSCs is enhanced independently of the NLRP3 inflammasome, we used inhibitors of components of the NLRP3 inflammasome, namely, Ac-YVAD-CHO, which inhibits caspase 1, and recombinant human IL-1 receptor antagonist (IL-1Ra), which antagonizes IL-1. Neither Ac-YVAD-CHO (10 μM) treatment nor recombinant human IL-1Ra (1 μg/ml) treatment during 2-D micromass culture prevented the formation of large cartilaginous masses (Figures 4A and B), *SOX9* upregulation (Figure 4C), or overproduction of GAG (Figure 4D) by chondrocytes derived from mutant iPSCs. The same was true when samples were treated

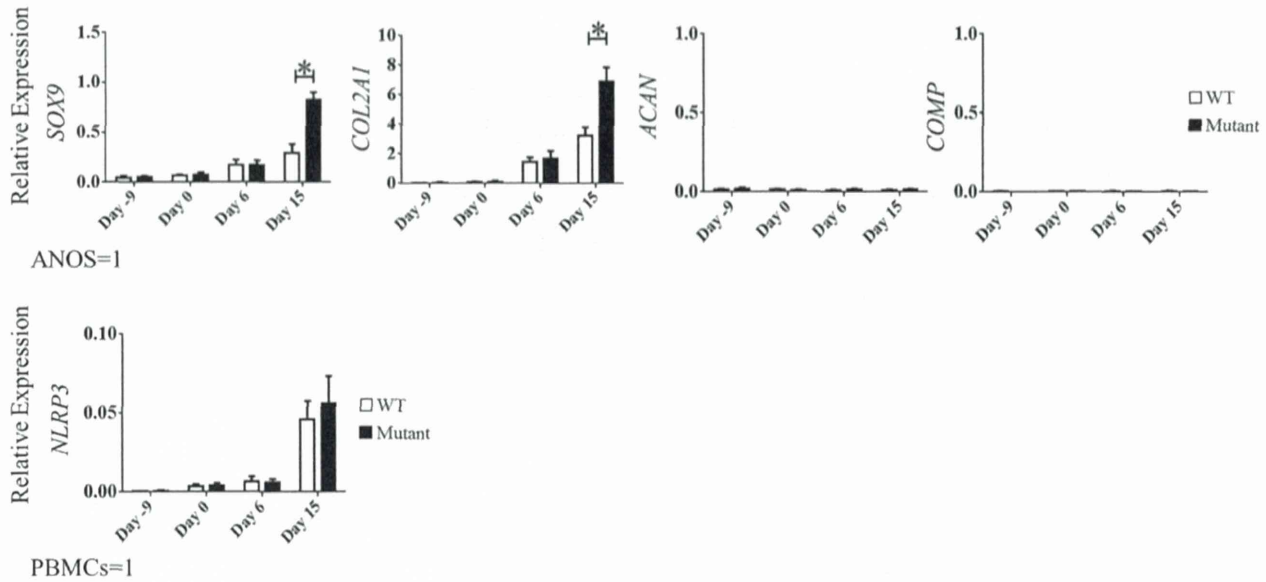

Figure 5. Up-regulation of the expression of *SOX9* and *COL2A1* in chondrocytes with mutated *NLRP3* during the chondroprogenitor cell stage. Expression of *SOX9*, *COL2A1*, *ACAN*, *COMP*, and *NLRP3* in each clone was measured in triplicate from day −9 to day 15 of chondrocyte differentiation of iPSCs from patients with neonatal-onset multisystem inflammatory disease with wild-type or mutant NLRP3. Expression levels of *SOX9*, *COL2A1*, *ACAN*, and *COMP* are shown relative to those in ANOS cells (set at 1), and the expression level of *NLRP3* is shown relative to that in peripheral blood mononuclear cells (PBMCs; set at 1). Bars show the mean ± SEM of 3 independent clones. Data are representative of 3 independent experiments with consistent results and were obtained using iPSCs from patient 1; similar results were obtained using iPSCs from patient 2. * = $P < 0.05$. See Figure 1 for other definitions.

with higher concentrations of these inhibitors (up to 1,000-fold higher) (data not shown). Taken together, these data strongly indicate that the enhanced chondrogenesis of mutant iPSCs is independent of caspase 1 and IL-1, and thus the NLRP3 inflammasome.

Correlation of the up-regulation of NLRP3 with the up-regulation of SOX9 in chondroprogenitor cells. To dissect the mechanism underlying the enhanced chondrogenesis of mutant iPSCs, we analyzed the time course of chondrocyte-specific gene expression in chondroprogenitor cells (Figure 5). Expression of *SOX9*, *COL2A1*, and *NLRP3* started to be up-regulated in chondroprogenitor cells on day 6. Importantly, on day 15, *SOX9* and *COL2A1* were up-regulated more in mutant chondroprogenitor cells than in wild-type chondroprogenitor cells, whereas *NLRP3* was up-regulated similarly in both types of cells (Figure 5). In contrast, at this time point, the other chondrocyte-specific markers *ACAN* and *COMP* were not expressed in either type of cell (Figure 5). Thus, differential up-regulation of *SOX9* in chondroprogenitor cells correlated with the up-regulation of *NLRP3* and preceded the up-regulation of *COMP* and *ACAN*.

Critical role of the CREB/ATF-binding site of the SOX9 promoter in mutated NLRP3–dependent enhancement of SOX9 expression. Next, we focused on *SOX9* because it was up-regulated together with *NLRP3*, and this preceded the up-regulation of other chondrocyte-specific markers. We analyzed the activity of the human *SOX9* promoter in chondroprogenitor cells in which the level of *SOX9* mRNA was increased. We created a luciferase reporter construct containing the 5′-UTR of human *SOX9*, which encompasses −927 to +84 bp of the transcription start site. This fragment has basal promoter activity and putative binding sites for 5 transcription factors, namely, NF-AT, activator protein 1 (AP-1), NF-κB, Sp1, and CREB/ATF (see Supplementary Figure 1, available on the *Arthritis & Rheumatology* web site at http://onlinelibrary.wiley.com/doi/10.1002/art.38912/abstract). This fragment showed no promoter activity in the monocytic cell line THP-1 or the erythroleukemic cell line K562, which do not express endogenous *SOX9* (data not shown). Importantly, human *SOX9* promoter activity was higher in mutant chondroprogenitor cells than in wild-type chondroprogenitor cells (Figure 6A). To identify the element of the human *SOX9*

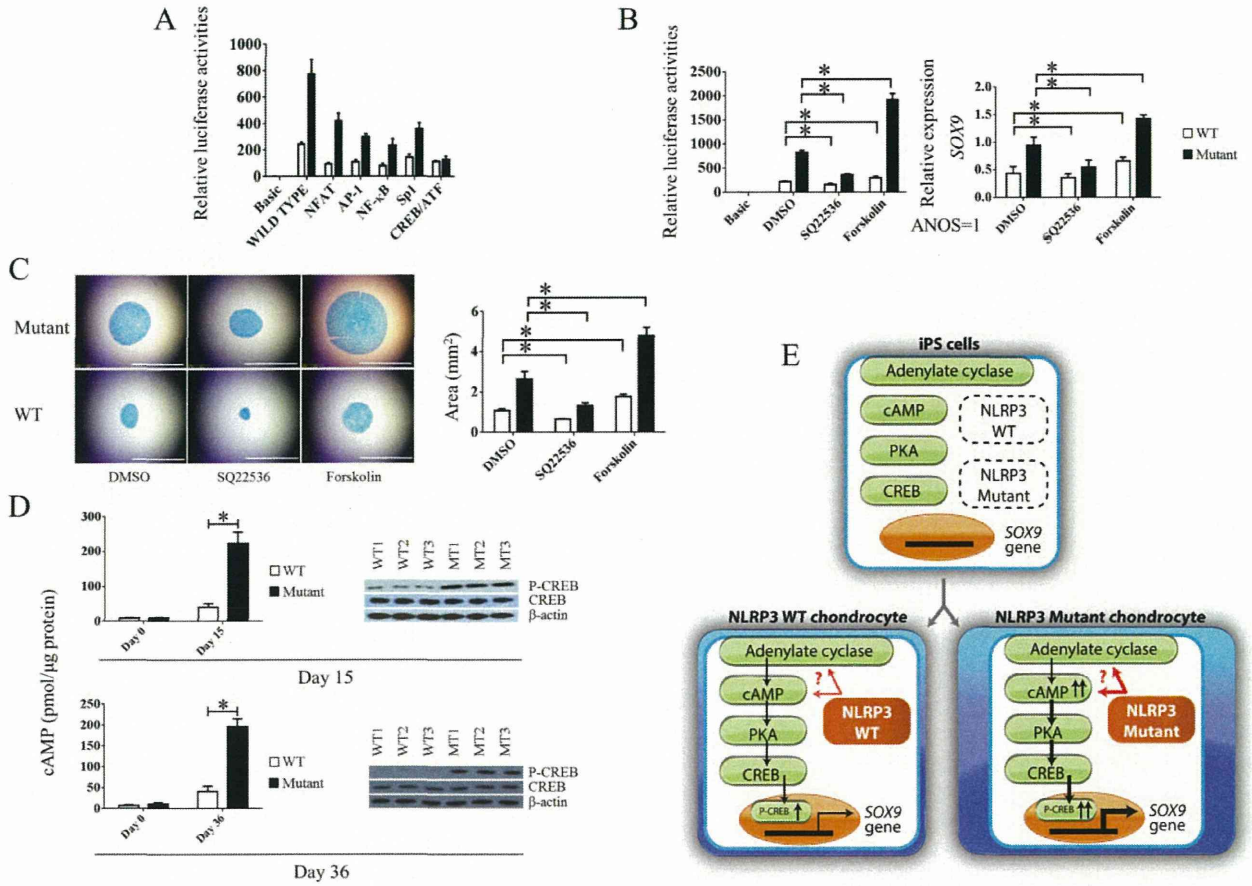

Figure 6. *SOX9* up-regulation in chondrocytes derived from iPSCs from patients with neonatal-onset multisystem inflammatory disease with mutant NLRP3 is dependent on the cAMP/protein kinase A (PKA)/CREB pathway. **A,** *SOX9* promoter activity in wild-type and mutant chondroprogenitor cells after the introduction of mutations into its transcription factor binding sites. **B,** *SOX9* promoter activity and expression in wild-type and mutant chondroprogenitor cells treated with SQ22536 or forskolin. **C,** Effects of SQ22536 and forskolin on 3-D pellets of mutant and wild-type cells. Both reagents were used at a concentration of 10 μM. Bars = 2.0 mm. **D,** Increased activity of the cAMP/PKA/CREB pathway in mutant chondroprogenitor cells compared to wild-type chondroprogenitor cells, as demonstrated by cAMP concentration in wild-type and mutant iPSCs (day 0) and chondroprogenitor cells (day 15 and day 36), and Western blot analysis of phosphorylated CREB in wild-type (WT1–3) and mutant (MT1–3) chondroprogenitor cells. **E,** Schematic diagram summarizing the molecular mechanism elucidated in this study. Bars in **A–D** show the mean ± SEM of 3 independent clones from which triplicate (**A, B,** and **D**) or duplicate (**C**) measurements were obtained. Data are representative of 2 independent experiments with consistent results and were obtained using iPSCs from patient 1; similar results were obtained using iPSCs from patient 2. * = $P < 0.05$. See Figure 1 for other definitions.

promoter region that responds in a mutated NLRP3–dependent manner, we performed site-directed mutagenesis of the sites of this promoter that bind the transcription factors NF-AT, AP-1, NF-κB, Sp1, and CREB/ATF (Supplementary Figure 1). Among the reporters with these mutations, the reporter that harbored a mutation in the CREB/ATF-binding site showed the least up-regulation of *SOX9* promoter activity in mutant cells (Figure 6A and Supplementary Figure 1). Thus, we speculate that the CREB/ATF-binding site is critical for activation of the human *SOX9* promoter in a mutated NLRP3–dependent manner.

Critical role of the cAMP/PKA/CREB pathway in SOX9 up-regulation caused by mutated NLRP3. To further explore the association between mutated NLRP3 and the cAMP/PKA/CREB pathway, we examined the effect of an adenylate cyclase activator and inhibitor (forskolin and SQ22536, respectively) on the activity of the human *SOX9* promoter and *SOX9* mRNA expression (Figure 6B). Among mutant chondroprogenitor

cells, *SOX9* promoter activity was 2.3-fold higher in forskolin-treated cells than in vehicle-treated cells, whereas *SOX9* promoter activity was 2-fold lower in SQ22536-treated cells than in vehicle-treated cells (Figure 6B). Similar effects were observed in wild-type chondroprogenitor cells, although they were less pronounced. These data correlated well with the effects of forskolin and SQ22536 on *SOX9* mRNA expression. We also examined the effects of forskolin and SQ22536 on 3-D chondrocyte pellet formation (Figure 6C). Compared to pellets of vehicle-treated mutant cells, pellets of mutant cells treated with forskolin and SQ22536 were 2.0-fold larger and 2.1-fold smaller, respectively. Similar effects were observed in wild-type cells, although they were less pronounced. These data clearly indicate that up-regulation of *SOX9* following activation of adenylate cyclase is involved in the enhanced chondrogenesis of mutant iPSCs.

We next measured the cAMP concentration to demonstrate that the activity of adenylate cyclase is increased in mutant chondroprogenitor cells. The concentration of cAMP was 4-fold higher in mutant chondroprogenitor cells than in wild-type chondroprogenitor cells on days 15 and 36 (Figure 6D). By contrast, the concentration of cAMP was similar in mutant and wild-type iPSCs, in which NLRP3 expression was low.

Finally, we examined the level of phosphorylated CREB in chondroprogenitor cells. CREB is phosphorylated by cAMP-activated PKA. According to Western blot analysis, the level of phosphorylated CREB was higher in mutant chondroprogenitor cells than in wild-type chondroprogenitor cells on days 15 and 36 (Figure 6D). Taken together, these data indicate that the cAMP/PKA/CREB pathway plays an important role in the up-regulation of *SOX9*, and therefore enhanced chondrogenesis, in chondroprogenitor cells with mutant NLRP3 (Figure 6E).

DISCUSSION

Disease-specific iPSCs have been used extensively to investigate the pathogenesis of diseases and to discover novel drugs. This approach is particularly useful to study rare diseases because tissues are often difficult to obtain from patients with such diseases. In this study, we used disease-specific iPSCs to study NOMID. Using this approach, we produced chondrocyte tissues with mutant and wild-type NLRP3, and revealed a previously unidentified connection between the inflammasome-associated molecule NLRP3 and the master regulator of chondrocyte differentiation SOX9.

SOX9 was up-regulated during the differentiation of iPSCs into chondrocytes, and this was particularly pronounced in mutant iPSCs. During cartilage development, SOX9 is highly expressed in immature chondrocytes and is required for the condensation and differentiation of mesenchymal cells. During the early stages of chondrogenesis, SOX9 activates the transcription of many cartilage-specific ECM genes, including *COL2A1*, *ACAN*, and *COMP*, by directly interacting with SOX5 and SOX6 (28,29). Overexpression of *SOX9* in chondrocytes using a recombinant adeno-associated virus significantly increases the synthesis of major ECM components in chondrocytes, without affecting their proliferation, in vivo and in vitro (30,31). In addition, retroviral transduction of SOX9 increases ECM production in human chondrocytes in vitro (32). These data correlate well with our observation that SOX9 overexpression driven by mutated NLRP3 caused overproduction of ECM, but did not increase chondrocyte proliferation.

It remains to be determined how enhanced expression of SOX9 in chondrocytes leads to epiphyseal overgrowth in NOMID patients. Conditional transgenic mice have been used to show that overexpression of *SOX9* in *COL2A1*-positive cells inhibits terminal differentiation of hypertrophic chondrocytes and endochondral bone formation (29). Although we have not directly confirmed the expression level of SOX9 in samples derived from NOMID patients, this previous study might help to link the findings of the present study with the clinical phenotype of NOMID patients.

We identified the cAMP/PKA/CREB pathway as being critical for the up-regulation of *SOX9* mRNA in a mutant NLRP3–dependent manner. cAMP is an intracellular second messenger that is involved in a variety of cellular processes (33). cAMP/PKA/CREB signaling is crucial in chondrogenesis, and synergism between cAMP and SOX9 is particularly important (34–36). Cotransfection of CREB binding protein (CBP) and p300 increases SOX9 activity (35). PKA phosphorylates SOX9 and thereby increases SOX9 activity, which results in the up-regulation of the *COL2A1* promoter through the interaction between CBP and SOX9 (34). In addition, the PKA inhibitor H89 blocks chondrogenesis in the chick limb bud (36). These data support the idea that cAMP/PKA/CREB signaling up-regulates SOX9 to enhance chondrogenesis.

Using stromal cells established from a tumor-like lesion in a NOMID patient, Almeida et al (37) demonstrated that activation of the cAMP/PKA/CREB pathway leads to caspase 1 activation, release of IL-1β, and

consequently the proliferation of bone stromal cells. This suggests that bone lesions in NOMID are caused in an NLRP3 inflammasome–dependent manner. One explanation for the discrepancy between their data and ours is that no disease-causing NLRP3 mutation was identified in the patient in that previous study; therefore, an unknown genetic alteration may have caused the NOMID phenotype. Another explanation is that different cell types were analyzed in the two studies. The previous study analyzed bone stromal cells established from a tumor-like lesion that might have been a heterogeneous population, while we focused on a single cell type, namely, chondrocytes.

The lack of environmental factors and interactions with other cell populations in our model might have eliminated some contributions of the NLRP3 inflammasome and IL-1β pathway that occur in NOMID patients. Furthermore, our observations relied on an artificial differentiation system in which iPSCs were first differentiated into cells of neural crest character and then into chondrocytes by culture in the presence of various exogenous factors. Abnormal epiphyseal growth is specifically observed around the knee joints of NOMID patients; therefore, additional events might be required to trigger abnormal chondrocyte proliferation in vivo. It is also possible that specific factors produced by surrounding cells in unaffected joints prevent mutant chondrocytes from manifesting their phenotype. Further analyses of patients or patient-derived samples would provide a better understanding of the pathophysiology of arthropathy in NOMID.

The interaction between cAMP and NLRP3 has been studied in monocyte/macrophages, in which the NLRP3 inflammasome is activated following binding of extracellular Ca^{2+} to Ca^{2+}-sensing receptors (CaSRs) (38,39). One study reported that an increase in extracellular Ca^{2+} is detected by CaSRs, which leads to phospholipase C activation and subsequently the release of Ca^{2+} from the endoplasmic reticulum and down-regulation of cAMP. cAMP binds directly to NLRP3 and inhibits assembly of the NLRP3 inflammasome. Therefore, this decrease in the level of intracellular cAMP relieves this inhibition and thereby induces activation of the NLRP3 inflammasome (38). On the other hand, another study reported that an increase in the extracellular Ca^{2+} concentration induces an increase in the intracellular Ca^{2+} concentration, thereby leading to activation of the NLRP3 inflammasome, and this mechanism requires the CaSRs GPRC6A and CaSR, but not the down-regulation of cAMP (39). Thus, the effects of cAMP on the NLRP3 inflammasome in monocyte/macrophages remain a subject of controversy.

In the chondrocyte differentiation system used in the present study, mutated NLRP3 caused SOX9 overexpression via the cAMP/PKA/CREB pathway, which is at odds with the relationship between cAMP and activation of the NLRP3 inflammasome in monocyte/macrophages. This discrepancy might be explained by the absence of other NLRP3 inflammasome components, such as ASC and procaspase 1, in the chondrocytes generated in the present study. Further analysis is needed to determine why cAMP/PKA/CREB signaling elicits different effects on mutated NLRP3 in chondrocytes and monocyte/macrophages, as well as how intracellular cAMP is up-regulated in chondrocytes derived from mutant iPSCs.

There have been many reports on the differentiation of chondrocytes from embryonic stem cells (ESCs) or iPSCs (40–42). However, previously, it was difficult to differentiate a sufficient number of chondrocytes with a relatively mature phenotype from ESCs or iPSCs, especially human ESCs or iPSCs. We have recently established a cartilage differentiation system in which iPSCs first differentiate into cells of neural crest character and then into chondrocytes, which enabled us to obtain a large number of chondrocytes with the phenotype of growth plate cartilage chondrocytes. An important aspect of the present study is that this differentiation system can generate a large number of chondrocytes that could share functional properties causing the arthropathy observed in NOMID. This system could thereby be used to screen for novel therapeutic agents.

In conclusion, we showed that SOX9 is overexpressed via the cAMP/PKA/CREB signaling pathway in chondrocytes with disease-causing mutations in NLRP3, and this causes overproduction of ECM independently of the NLRP3 inflammasome. We used iPSC technology to elucidate the role of chondrocytes in the pathophysiology of the human disease NOMID.

ACKNOWLEDGMENTS

We are grateful to K. Hayakawa, M. Fukuta, S. Nagata, and M. Hiraga of Kyoto University for technical assistance and to N. Kambe of Chiba University for critical reading of the manuscript.

AUTHOR CONTRIBUTIONS

All authors were involved in drafting the article or revising it critically for important intellectual content, and all authors approved the final version to be published. Drs. Nishikomori and Toguchida had

full access to all of the data in the study and take responsibility for the integrity of the data and the accuracy of the data analysis.
Study conception and design. Yokoyama, Ikeya, Tanaka, Nishikomori, Nakayama, Nakahata, Heike, Toguchida.
Acquisition of data. Yokoyama, Umeda, Nodomi, Horigome, Kusaka, Ohara.
Analysis and interpretation of data. Yokoyama, Umeda, Oda, Nodomi, Nasu, Matsumoto, Izawa, Kusaka, Saito, Yasumi, Nishikomori, Ohara.

ADDITIONAL DISCLOSURES

Author Horigome is an employee of Dainippon Sumitomo Pharma.

REFERENCES

1. Kufer TA, Sansonetti PJ. NLR functions beyond pathogen recognition. Nat Immunol 2011;12:121–8.
2. Hoffman HM, Mueller JL, Broide DH, Wanderer AA, Kolodner RD. Mutation of a new gene encoding a putative pyrin-like protein causes familial cold autoinflammatory syndrome and Muckle-Wells syndrome. Nat Genet 2001;29:301–5.
3. Tanaka N, Izawa K, Saito MK, Sakuma M, Oshima K, Ohara O, et al. High incidence of NLRP3 somatic mosaicism in patients with chronic infantile neurologic, cutaneous, articular syndrome: results of an international multicenter collaborative study. Arthritis Rheum 2011;63:3625–32.
4. Feldmann J, Prieur AM, Quartier P, Berquin P, Certain S, Cortis E, et al. Chronic infantile neurological cutaneous and articular syndrome is caused by mutations in CIAS1, a gene highly expressed in polymorphonuclear cells and chondrocytes. Am J Hum Genet 2002;71:198–203.
5. Latz E, Xiao TS, Stutz A. Activation and regulation of the inflammasomes. Nat Rev Immunol 2013;13:397–411.
6. Gattorno M, Martini A. Beyond the NLRP3 inflammasome: autoinflammatory diseases reach adolescence [review]. Arthritis Rheum 2013;65:1137–47.
7. Bauernfeind FG, Horvath G, Stutz A, Alnemri ES, MacDonald K, Speert D, et al. NF-κB activating pattern recognition and cytokine receptors license NLRP3 inflammasome activation by regulating NLRP3 expression. J Immunol 2009;183:787–91.
8. Mariathasan S, Weiss DS, Newton K, McBride J, O'Rourke K, Roose-Girma M, et al. Cryopyrin activates the inflammasome in response to toxins and ATP. Nature 2006;440:228–32.
9. Hoffman HM, Rosengren S, Boyle DL, Cho JY, Nayar J, Mueller JL, et al. Prevention of cold-associated acute inflammation in familial cold autoinflammatory syndrome by interleukin-1 receptor antagonist. Lancet 2004;364:1779–85.
10. Hawkins PN, Lachmann HJ, McDermott MF. Interleukin-1-receptor antagonist in the Muckle-Wells syndrome. N Engl J Med 2003;348:2583–4.
11. Lachmann HJ, Kone-Paut I, Kuemmerle-Deschner JB, Leslie KS, Hachulla E, Quartier P, et al. Use of canakinumab in the cryopyrin-associated periodic syndrome. N Engl J Med 2009;360:2416–25.
12. Arostegui JI, Lopez Saldana MD, Pascal M, Clemente D, Aymerich M, Balaguer F, et al. A somatic NLRP3 mutation as a cause of a sporadic case of chronic infantile neurologic, cutaneous, articular syndrome/neonatal-onset multisystem inflammatory disease: novel evidence of the role of low-level mosaicism as the pathophysiologic mechanism underlying Mendelian inherited diseases. Arthritis Rheum 2010;62:1158–66.
13. Hill SC, Namde M, Dwyer A, Poznanski A, Canna S, Goldbach-Mansky R. Arthropathy of neonatal onset multisystem inflammatory disease (NOMID/CINCA). Pediatr Radiol 2007;37:145–52.
14. Mackie EJ, Tatarczuch L, Mirams M. The skeleton: a multifunctional complex organ. The growth plate chondrocyte and endochondral ossification. J Endocrinol 2011;211:109–21.
15. Goldring MB, Tsuchimochi K, Ijiri K. The control of chondrogenesis. J Cell Biochem 2006;97:33–44.
16. Bonar SL, Brydges SD, Mueller JL, McGeough MD, Pena C, Chen D, et al. Constitutively activated NLRP3 inflammasome causes inflammation and abnormal skeletal development in mice. PloS One 2012;7:e35979.
17. Tanaka T, Takahashi K, Yamane M, Tomida S, Nakamura S, Oshima K, et al. Induced pluripotent stem cells from CINCA syndrome patients as a model for dissecting somatic mosaicism and drug discovery. Blood 2012;120:1299–308.
18. Umeda K, Zhao J, Simmons P, Stanley E, Elefanty A, Nakayama N. Human chondrogenic paraxial mesoderm, directed specification and prospective isolation from pluripotent stem cells. Sci Rep 2012;2:455.
19. Nasu A, Ikeya M, Yamamoto T, Watanabe A, Jin Y, Matsumoto Y, et al. Genetically matched human iPS cells reveal that propensity for cartilage and bone differentiation differs with clones, not cell type of origin. PloS One 2013;8:e53771.
20. Sakai H, Okafuji I, Nishikomori R, Abe J, Izawa K, Kambe N, et al. The CD40-CD40L axis and IFN-γ play critical roles in Langhans giant cell formation. Int Immunol 2012;24:5–15.
21. Aoyama T, Okamoto T, Nagayama S, Nishijo K, Ishibe T, Yasura K, et al. Methylation in the core-promoter region of the chondromodulin-I gene determines the cell-specific expression by regulating the binding of transcriptional activator Sp3. J Biol Chem 2004;279:28789–97.
22. Ushita M, Saito T, Ikeda T, Yano F, Higashikawa A, Ogata N, et al. Transcriptional induction of SOX9 by NF-κB family member RelA in chondrogenic cells. Osteoarthritis Cartilage 2009;17:1065–75.
23. Kajita Y, Kato T Jr, Tamaki S, Furu M, Takahashi R, Nagayama S, et al. The transcription factor Sp3 regulates the expression of a metastasis-related marker of sarcoma, actin filament-associated protein 1-like 1 (AFAP1L1). PloS One 2013;8:e49709.
24. Sandelin A, Alkema W, Engstrom P, Wasserman WW, Lenhard B. JASPAR: an open-access database for eukaryotic transcription factor binding profiles. Nucleic Acids Res 2004;32:D91–4.
25. Saito M, Fujisawa A, Nishikomori R, Kambe N, Nakata-Hizume M, Yoshimoto M, et al. Somatic mosaicism of CIAS1 in a patient with chronic infantile neurologic, cutaneous, articular syndrome. Arthritis Rheum 2005;52:3579–85.
26. Saito M, Nishikomori R, Kambe N, Fujisawa A, Tanizaki H, Takeichi K, et al. Disease-associated CIAS1 mutations induce monocyte death, revealing low-level mosaicism in mutation-negative cryopyrin-associated periodic syndrome patients. Blood 2008;111:2132–41.
27. Aksentijevich I, Nowak M, Mallah M, Chae JJ, Watford WT, Hofmann SR, et al. De novo CIAS1 mutations, cytokine activation, and evidence for genetic heterogeneity in patients with neonatal-onset multisystem inflammatory disease (NOMID): a new member of the expanding family of pyrin-associated autoinflammatory diseases. Arthritis Rheum 2002;46:3340–8.
28. Akiyama H, Lefebvre V. Unraveling the transcriptional regulatory machinery in chondrogenesis. J Bone Miner Metab 2011;29:390–5.
29. Kim Y, Murao H, Yamamoto K, Deng JM, Behringer RR, Nakamura T, et al. Generation of transgenic mice for conditional overexpression of Sox9. J Bone Miner Metab 2011;29:123–9.
30. Cucchiarini M, Orth P, Madry H. Direct rAAV SOX9 administration for durable articular cartilage repair with delayed terminal differentiation and hypertrophy in vivo. J Mol Med (Berlin) 2013;91:625–36.
31. Cucchiarini M, Thurn T, Weimer A, Kohn D, Terwilliger EF, Madry H. Restoration of the extracellular matrix in human

osteoarthritic articular cartilage by overexpression of the transcription factor SOX9. Arthritis Rheum 2007;56:158–67.
32. Tew SR, Li Y, Pothacharoen P, Tweats LM, Hawkins RE, Hardingham TE. Retroviral transduction with SOX9 enhances re-expression of the chondrocyte phenotype in passaged osteoarthritic human articular chondrocytes. Osteoarthritis Cartilage 2005;13:80–9.
33. Carroll SH, Ravid K. Differentiation of mesenchymal stem cells to osteoblasts and chondrocytes: a focus on adenosine receptors. Expert Rev Mol Med 2013;15:e1.
34. Huang W, Zhou X, Lefebvre V, de Crombrugghe B. Phosphorylation of SOX9 by cyclic AMP-dependent protein kinase A enhances SOX9's ability to transactivate a Col2a1 chondrocyte-specific enhancer. Mol Cell Biol 2000;20:4149–58.
35. Tsuda M, Takahashi S, Takahashi Y, Asahara H. Transcriptional co-activators CREB-binding protein and p300 regulate chondrocyte-specific gene expression via association with Sox9. J Biol Chem 2003;278:27224–9.
36. Yoon YM, Oh CD, Kang SS, Chun JS. Protein kinase A regulates chondrogenesis of mesenchymal cells at the post-precartilage condensation stage via protein kinase C-α signaling. J Bone Miner Res 2000;15:2197–205.
37. Almeida MQ, Tsang KM, Cheadle C, Watkins T, Grivel JC, Nesterova M, et al. Protein kinase A regulates caspase-1 via Ets-1 in bone stromal cell-derived lesions: a link between cyclic AMP and pro-inflammatory pathways in osteoblast progenitors. Hum Mol Genet 2011;20:165–75.
38. Lee GS, Subramanian N, Kim AI, Aksentijevich I, Goldbach-Mansky R, Sacks DB, et al. The calcium-sensing receptor regulates the NLRP3 inflammasome through Ca^{2+} and cAMP. Nature 2012;492:123–7.
39. Rossol M, Pierer M, Raulien N, Quandt D, Meusch U, Rothe K, et al. Extracellular Ca^{2+} is a danger signal activating the NLRP3 inflammasome through G protein-coupled calcium sensing receptors. Nat Commun 2012;3:1329.
40. Barberi T, Willis LM, Socci ND, Studer L. Derivation of multipotent mesenchymal precursors from human embryonic stem cells. PLoS Med 2005;2:e161.
41. Kawaguchi J, Mee PJ, Smith AG. Osteogenic and chondrogenic differentiation of embryonic stem cells in response to specific growth factors. Bone 2005;36:758–69.
42. Zur Nieden NI, Kempka G, Rancourt DE, Ahr HJ. Induction of chondro-, osteo- and adipogenesis in embryonic stem cells by bone morphogenetic protein-2: effect of cofactors on differentiating lineages. BMC Dev Biol 2005;5:1.

PLOS | ONE

RESEARCH ARTICLE

Derivation of Mesenchymal Stromal Cells from Pluripotent Stem Cells through a Neural Crest Lineage using Small Molecule Compounds with Defined Media

Makoto Fukuta[1,2,3☯], Yoshinori Nakai[4☯], Kosuke Kirino[5☯], Masato Nakagawa[6], Kazuya Sekiguchi[1,2,7], Sanae Nagata[2], Yoshihisa Matsumoto[1,2,3], Takuya Yamamoto[6,8], Katsutsugu Umeda[9], Toshio Heike[9], Naoki Okumura[10], Noriko Koizumi[10], Takahiko Sato[4], Tatsutoshi Nakahata[5], Megumu Saito[5], Takanobu Otsuka[3], Shigeru Kinoshita[4], Morio Ueno[4]*, Makoto Ikeya[2]*, Junya Toguchida[1,2,7]*

1. Department of Tissue Regeneration, Institute for Frontier Medical Sciences, Kyoto University, Kyoto, Japan, **2.** Department of Cell Growth and Differentiation, Center for iPS Cell Research and Application, Kyoto University, Kyoto, Japan, **3.** Department of Orthopaedic Surgery, Graduate School of Medical Sciences, Nagoya City University, Nagoya, Japan, **4.** Department of Ophthalmology, Kyoto Prefectural University of Medicine, Kyoto, Japan, **5.** Department of Clinical Application, Center for iPS Cell Research and Application, Kyoto University, Kyoto, Japan, **6.** Department of Reprogramming Science, Center for iPS Cell Research and Application, Kyoto University, Kyoto, Japan, **7.** Department of Orthopaedic Surgery, Graduate School of Medicine, Kyoto University, Kyoto, Japan, **8.** Institute for Integrated Cell-Material Sciences (WPI-iCeMS), Kyoto University, Kyoto, Japan, **9.** Department of Pediatrics, Graduate School of Medicine, Kyoto University, Kyoto, Japan, **10.** Department of Biomedical Engineering, Faculty of Life and Medical Sciences, Doshisha University, Kyotanabe, Japan

*mueno@koto.kpu-m.ac.jp (MU); mikeya@cira.kyoto-u.ac.jp (MI); togjun@frontier.kyoto-u.ac.jp (JT)

☯ These authors contributed equally to this work.

Citation: Fukuta M, Nakai Y, Kirino K, Nakagawa M, Sekiguchi K, et al. (2014) Derivation of Mesenchymal Stromal Cells from Pluripotent Stem Cells through a Neural Crest Lineage using Small Molecule Compounds with Defined Media. PLoS ONE 9(12): e112291. doi:10.1371/journal.pone.0112291

Editor: Maurilio Sampaolesi, Stem Cell Research Institute, Belgium

Received: March 24, 2014

Accepted: October 6, 2014

Published: December 2, 2014

Funding: This work was supported in part by Grants-in-Aid for Scientific Research from JSPS (#25293320), a grant from Core Center for iPS Cell Research, Research Center Network for Realization of Regenerative Medicine from JST, and the Leading Project for Realization of Regenerative Medicine from MEXT to MI and JT. MI was also supported by the Adaptable and Seamless Technology Transfer Program through target-driven R&D, Exploratory Research from JST (AS242Z00931P). JT was also supported by the Center for Clinical Application Research on Specific Disease/Organ from JST. MU was also supported by Grants-in-Aid for Scientific Research from JSPS (#20791288). The funders had no role in the study design, data collection and analysis, decision to publish, or preparation of the manuscript.

Competing Interests: The authors have declared that no competing interests exist.

Abstract

Neural crest cells (NCCs) are an embryonic migratory cell population with the ability to differentiate into a wide variety of cell types that contribute to the craniofacial skeleton, cornea, peripheral nervous system, and skin pigmentation. This ability suggests the promising role of NCCs as a source for cell-based therapy. Although several methods have been used to induce human NCCs (hNCCs) from human pluripotent stem cells (hPSCs), such as embryonic stem cells (ESCs) and induced pluripotent stem cells (iPSCs), further modifications are required to improve the robustness, efficacy, and simplicity of these methods. Chemically defined medium (CDM) was used as the basal medium in the induction and maintenance steps. By optimizing the culture conditions, the combination of the GSK3β inhibitor and TGFβ inhibitor with a minimum growth factor (insulin) very efficiently induced hNCCs (70–80%) from hPSCs. The induced hNCCs expressed cranial NCC-related genes and stably proliferated in CDM supplemented with EGF and FGF2 up to at least 10

passages without changes being observed in the major gene expression profiles. Differentiation properties were confirmed for peripheral neurons, glia, melanocytes, and corneal endothelial cells. In addition, cells with differentiation characteristics similar to multipotent mesenchymal stromal cells (MSCs) were induced from hNCCs using CDM specific for human MSCs. Our simple and robust induction protocol using small molecule compounds with defined media enabled the generation of hNCCs as an intermediate material producing terminally differentiated cells for cell-based innovative medicine.

Introduction

In order to apply human pluripotent stem cells (hPSCs) to innovative medicine, such as cell therapy, disease modeling, and drug discovery, robust and efficient methods to produce the desired cell types without contaminating undesired cells are indispensable [1]. Since the contamination of hPSCs, in particular, may cause serious adverse effects, careful monitoring, which requires a considerable amount of time and cost, has to be conducted. Therefore, it would be beneficial to have intermediate cells between hPSCs and terminally differentiated cells, which are proved to have no contaminated hPSCs, contain limited but multiple differentiation properties, and stably proliferate without phenotypic changes. One of the promising candidates with such features is the neural crest cell (NCC) [2].

The neural crest emerges at the border of the neural and non-neural ectoderm in gastrula embryos during vertebrate development [3]. Cells in the neural crest, and later in the dorsal part of the neural tube, eventually delaminate and migrate throughout the body while retaining their characteristic phenotype [4]. When they reach their target tissues, NCCs differentiate into specific cell types depending on the location [5]. NCCs give rise to the majority of cranial bone, cartilage, smooth muscle, and pigmented cells in the cranial region, as well as neurons and glia in the peripheral nervous system [3–5]. Cardiac NCCs are known to contribute to valves in the heart, while vagal NCCs differentiate into enteric ganglia in the gut [6]. NCCs give rise to neurons and glia in the peripheral nervous system in the trunk region, secretory cells in the endocrine system, and pigmented cells in the skin.

Using a lineage-tracing system, rodent neural crest-derived cells were detected in adult tissues such as bone marrow, and still retained multipotent differentiation properties, which indicated that these cells are one of the cell-of-origin of multipotent mesenchymal stromal cells (MSCs) [7, 8]. Therefore, the production of human MSCs (hMSCs) from hPSCs via NCC lineage is a promising approach for the use of hPSCs in innovative medicine [9, 10]. A considerable number of studies have been dedicated to establishing robust and efficient induction methods from hPSCs to hNCCs in the past decade [11–13]. However, most of these studies used non-human stromal feeder cells or only achieved low induction

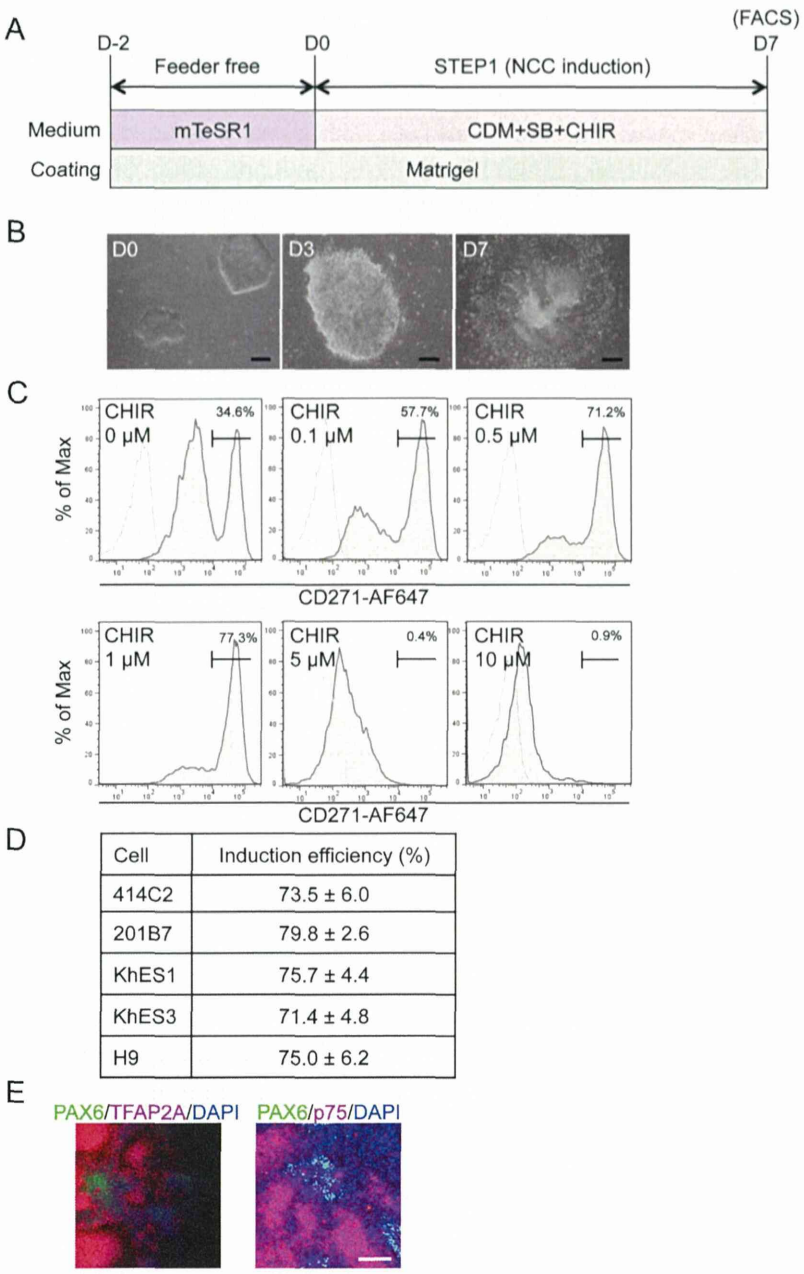

Cell	Induction efficiency (%)
414C2	73.5 ± 6.0
201B7	79.8 ± 2.6
KhES1	75.7 ± 4.4
KhES3	71.4 ± 4.8
H9	75.0 ± 6.2

Figure 1. Induction of p75^{high} cells from hPSCs. A) Schematic representation of the protocol. B) Morphology of colonies during the induction. Phase contrast images were taken on days 0, 3, and 7. Scale bar, 200 μm. C) The fraction of p75-positive cells in 201B7 cells was treated with SB431542 (SB) (10 μM) and CHIR99021 (CHIR) (indicated concentration) for seven days, stained with an anti-p75 antibody, and analyzed by FACS. D) Fraction of the p75^{high} population induced by SB (10 μM) and CHIR (1 μM) from hESCs (KhES1, KhES3, H9) and hiPSCs (414C2, 201B7). Average ± SD. N=3, biological triplicate. E) Immunocytochemical analyses of colonies on day 7 (201B7). Cells were stained with antibodies against PAX6, TFAP2A, and p75. Scale bar, 100 μm.

doi:10.1371/journal.pone.0112291.g001

efficiencies. An ideal method from the standpoint of clinical applications is free from xeno-materials, such as feeder cells or serum, and can be performed using a chemically defined medium (CDM). Two groups have published protocols that are compatible with these requirements [14, 15]. The first group employed a two-step approach, in which hPSCs were firstly dissociated into single cells and cultured with CDM for two weeks for the adaptation. Cells were then cultured with CDM that was supplemented with an activator of Wnt signaling and inhibitor of Activin/Nodal/TGFβ signaling, but was free from BMP signaling modulation [14]. The other group used MEF-conditioned hESC media for the initial step, and replaced it with knockout serum replacement (KSR)-based medium, which thereafter was gradually replaced with an increasing amount of N2 media. They employed an inhibitor for BMP signaling in addition to an inhibitor for Activin/Nodal/TGFβ signaling during the initial 3 days, and then replaced them with an activator of Wnt signaling [15]. Therefore, the requirement for signal modulators, particularly BMP signaling inhibitors, remains controversial. Further modifications are still needed to improve the robustness, efficacy, and simplicity of these methods.

We here developed a robust and efficient induction protocol using CDM containing inhibitors for TGFβ signaling and GSK3β, but not for BMP signaling with minimal growth factors. The protocol very efficiently induced hNCCs (70–80%) from hPSCs irrespective of the type (hESCs vs hiPSCs) or generating method (viral-integrated vs plasmid-episomal). Genome-wide analyses revealed that induced hNCCs retained their gene expression profile as NCCs even after 10 passages. As for differentiation properties, induced hNCCs successfully differentiated into peripheral neurons, glia, melanocytes and corneal endothelial cells. In addition, induced hNCCs were able to produce cells comparable to hMSCs, which were free from contaminated hPSCs and could differentiate into osteo-, chondro-, and adipogenic cells. Furthermore, using iPSCs generated and maintained under feeder-free and xeno-free culture systems, we successfully induced hNCCs, hMSCs, and osteogenic cells using chemically defined media.

Materials and Methods

Ethics statement

The experimental protocols dealing human subjects were approved by the Ethics Committee of the Department of Medicine and Graduate School of Medicine, Kyoto University. Written informed consent was provided by each donor.

Cell lines

hESCs (H9, KhES1, and KhES3) and hiPSCs (414C2 and 201B7) were used in this study [16–19] They were maintained on SNL feeder cells [20] in Primate ES cell medium (ReproCELL, Tokyo, Japan) supplemented with 4 ng/ml recombinant human FGF2 (WAKO, Osaka, Japan). 987A3, hiPSCs generated and maintained

under feeder-free and xeno-free culture systems from human primary fibroblasts, were maintained on iMatrix-551 (rLN511E) (Nippi, Tokyo, Japan)-coated cell culture plates with StemFit (Ajinomoto, Tokyo, Japan) as described previously [21]. Bone marrow derived hMSCs were obtained from donors and used in our previous study [22]. Human corneal endothelial cells were isolated from human corneal tissues obtained for research purpose from SightLife (Seattle, WA, USA).

Culture media and reagents

mTeSR1 medium (STEMCELL Technology, Vancouver, Canada) was used for the feeder-free culture of PSCs. The induction and maintenance of hNCCs were performed using previously reported CDM [23], which contains Iscove's modified Dulbecco's medium/Ham's F-12 1:1, 1x chemically defined lipid concentrate (GIBCO, Grand Island, NY, USA), 15 μg/ml apo-transferrin (Sigma, St. Louis, MO, USA), 450 μM monothioglycerol (Sigma), 5 mg/ml purified BSA (99% purified by crystallization; Sigma), 7 μg/ml Insulin (WAKO), and penicillin/streptomycin (Invitrogen, Carlsbad, CA, USA). Culture dishes were coated with growth factor-reduced Matrigel (BD, Bedford, MA, USA) or fibronectin (Millipore, Bedford, CA, USA). EGF (R&D, Minneapolis, USA) and FGF2 were used to maintain hNCCs [24]. SB431542 (SB) (Sigma), CHIR99021 (CHIR) (WAKO), BMP4 (R&D), DMH1 (Tocris, Bristol, UK), LDN193189 (Stemgent, Cambridge, MA, USA), and recombinant human Noggin (R&D) were used to modulate growth factor signals. Retinoic acid (RA) (Sigma) was used to modulate hNCCs.

Fluorescence-Activated Cell Sorting (FACS)

FACS was performed by AriaII (BD) according to the manufacturer's protocol. The antibodies used in FACS were listed in Table S1. In all experiments, FACS histograms of isotype controls were similar to those without antibodies; therefore, histograms without antibodies were used as control populations.

Immunocyto- and immunohistochemistry

Prior to performing immunostaining with antibodies, cells on plates were fixed with 4% paraformaldehyde at 4℃ for 15 minutes, washed two times with PBS, and incubated with 0.3% TritonX100 at 4℃ for 30 minutes as the surface-active agent for penetration processing, and any nonspecific binding was blocked with 2% skim milk/PBS at 4℃ for 1 hour. Cornea samples obtained from rabbits euthanized three days after the injection of cells were fixed with 4% paraformaldehyde and incubated in 1% bovine serum albumin (BSA) (Sigma) to block other bindings. DAPI (1:5000; Sigma) was used to counterstain nuclei. The primary antibodies used in this study were summarized in Table S1. The observation and assessment of samples were performed with BZ-9000E (Keyence, Osaka, Japan).

RT-PCR and qPCR

Total RNA was purified with the RNeasy Mini kit (Qiagen, Valencia, CA, USA) and treated with the DNase-one kit (Qiagen) to remove genomic DNA. One microgram of total RNA was reverse transcribed for single-stranded cDNA using a random primer and Superscript III reverse transcriptase (Invitrogen), according to the manufacturer's instructions. PCR was performed with ExTaq (Takara, Shiga, Japan). Quantitative PCR with the Thunderbird SYBR qPCR Mix (TOYOBO, Osaka, Japan) was performed using the StepOne real-time PCR system (Applied Biosystems, Forester City, CA, USA) in duplicate or triplicate. Primer sequences were listed in Table S2.

cDNA microarray

Total RNA was prepared using the RNeasy Mini Kit (Qiagen). cDNA was synthesized using the GeneChip WT (Whole Transcript) Sense Target Labeling and Control Reagents kit as described by the manufacturer (Affymetrix, Santa Clara, CA, USA). Hybridization to the GeneChip Human Gene 1.0 ST expression arrays, washing, and scanning were performed according to the manufacturer's protocol (Affymetrix). Expression values were calculated using the RMA summarization method and the data obtained were analyzed by GeneSpring GX 11.5.6 (Agilent Technologies, Santa Clara, CA, USA) for correlation coefficients, scatter plots, a volcano plot, heat maps, and hierarchical clustering (Distance metrics: Pearson's Centered, Linkage rule: Average). Differentially expressed genes were identified by statistical analyses and fold changes. Statistical analyses were performed using a one-way ANOVA with a Benjamini and Hochberg False Discovery Rate (BH-FDR =0.01) multiple testing correction followed by Tukey HSD post hoc tests (GeneSpring GX). Microarray data have been submitted to the Gene Expression Omnibus (GEO) public database at NCBI, and the accession number is GSE 60313. Data for hBM90, 91, and 94 have already been described [22]. Data from GSE44727 and GSE45223 were used for a comparison analysis in Figure S3.

Differentiation of hPSC-derived hNCCs

Peripheral neuronal differentiation

Sorted hNCCs were cultured in CDM supplemented with 10 μM SB and 1 μM CHIR as a sphere using the hanging drop technique (1×10^4 cells per sphere) as previously described [25]. Twenty-four hours after the hanging drop culture, spheres were plated onto Polyornithine/laminin/fibronectin (PO/Lam/FN)-coated plates in DMEM/F12 (Invitrogen) supplemented with 1 x N2 supplement (GIBCO), 1 x GlutaMAX (Invitrogen), 20 ng/ml FGF2, and 20 ng/ml EGF. These cells were cultured for two days under these conditions and the medium was then replaced with DMEM/F12 supplemented with 1 x N2 supplement, 1 x GlutaMAX, and 10 ng/ml BDNF (R&D), GDNF (R&D), NT-3 (R&D), and NGF (R&D). The medium was changed every 3 days and passages were performed every week [26].

Differentiation was confirmed by immunostaining for peripherin, Tuj-1, and GFAP 3 weeks after induction.

Melanocyte differentiation

Cells were plated onto fibronectin-coated dishes in CDM supplemented with 10 μM SB and 1 μM CHIR. Melanocyte induction was performed the next day with CDM supplemented with 1 μM CHIR, 25 ng/ml BMP4, and 100 nM endothelin-3 (American Peptide Company, Sunnyvale, CA, USA) [15, 27, 28]. The medium was changed every other day. Differentiation was confirmed by induction of the *MITF* and *c-KIT* genes on day 7.

Corneal endothelial cell differentiation

Cells were induced to corneal endothelial cells with corneal endothelial cell-conditioned CDM. Conditioned CDM was derived by collecting medium from cultured human corneal endothelial cells [29]. The selective ROCK inhibitor Y-27632 (WAKO) was used on the first day of the induction. The medium was changed every two days, and cells were analyzed by immunocytochemistry after twelve days. RT-qPCR was performed 3, 5, and 8 days after the induction.

Induction of hMSCs from hNCCs

Cells were plated onto tissue culture dishes (BD) at a density of 6.5×10^4 cell/cm^2 in CDM supplemented with 10 μM SB and 1 μM CHIR. The medium was replaced the next day with αMEM (Nacalai Tesque, Tokyo, Japan) supplemented with 10% fetal bovine serum (FBS) (Nichirei Inc., Tokyo, Japan) [14, 26]. The morphology of cells started to change approximately 4 days after the induction. Passages were performed every week using 0.25% trypsin-EDTA (GIBCO) at a density of 1×10^4 cells/cm^2. hMSC markers (CD73, CD44, CD45 and CD105) were analyzed by FACS 14 days after the hMSC induction. We used STK2 (DS Pharma Biomedical, Osaka, Japan) as the MSC medium and tissue culture dishes coated with fibronectin for the hMSC induction under chemically defined media conditions.

Differentiation of hNCC-derived hMSCs

Osteogenic differentiation

A total of 2.5×10^5 induced hMSCs/well were seeded on 6-well dishes (BD) and cultured in osteogenic induction medium, αMEM, 10% FBS, 0.1 μM dexamethasone, 50 μg/ml ascorbic acid, and 10 mM β-glycerophosphate for 2 weeks for osteogenic differentiation [24]. STK3 (DS Pharma) was used as the osteogenic induction medium instead of the osteogenic induction medium to achieve osteogenic differentiation under chemically defined media conditions. The culture medium was changed every other day for 1 week. Differentiation properties were confirmed by the formation of calcified nodules, as detected with Alizarin Red staining. Briefly, culture wells were washed twice in phosphate-buffered saline (PBS) and fixed for 10 minutes at room temperature in 100% ethyl alcohol. The

Alizarin Red solution (40 mM, pH 4.2) was applied to the fixed wells for 10 min at room temperature. Non-specific staining was removed by several washes with water.

Chondrogenic differentiation

Two-dimensional chondrogenic induction was performed as previously described [30]. Briefly, cells (1.5×10^5) that induced hMSCs were suspended in 5 μl of chondrogenic medium (DMEM: F12 (Invitrogen), 1% (v/v) ITS1 mix (BD), 0.17 mM AA2P, 0.35 mM Proline (Sigma), 0.1 mM dexamethasone (Sigma), 0.15% (v/v) glucose (Sigma), 1 mM Na-pyruvate (Invitrogen), 2 mM GlutaMax, and 0.05 mM MTG supplemented with 40 ng/ml PDGF-BB and 1% (v/v) FBS (Nichirei)), and were subsequently transferred to fibronectin-coated 24-well plates (BD). A total of 1 ml of the chondrogenic medium was added after 1 hour. TGFβ3 (R&D) was subsequently added at 10 ng/ml on days 3 to 6, and BMP4 was added to a concentration of 50 ng/ml on day 10. Micromass cultures were maintained at 37℃ under 5% CO_2 and 5% O_2 for 16 days. Differentiation properties were confirmed by Alcian Blue staining. Briefly, induced cells were fixed for 30 minutes with 10% formalin (Sigma) and rinsed with PBS. These cells were then stained overnight with Alcian Blue solution (1% Alcian Blue (MUTO PURE CHEMICAL CO., LTD, Tokyo, Japan) in 3% glacial acetic and 1% HCl, pH 1) and destained with the acetic acid solution.

Adipogenic differentiation

Cells were seeded onto 6-well tissue culture dishes at a density of 5.0×10^5 cells/well for adipogenic differentiation, and were cultured in αMEM containing 10% FBS, 1 mM dexamethasone, 10 mg/ml insulin, and 0.5 mM isobutylxanthine for 3 weeks [31]. Induced cells were fixed in 10% formalin for 1 hour at room temperature, followed by 20 minutes in 0.3% Oil Red O staining solution (Sigma).

Results

Derivation of $p75^{high}$ cells from hPSCs

To transfer hPSCs from feeder to feeder-free culture conditions, colonies were dissociated into small cell clumps (about 10 cells/clumps) by pipetting several times, seeded on matrigel-coated dishes (2–4 clumps/cm^2), and cultured with mTeSR1 medium for two days. hNCC induction was then initiated by substituting CDM supplemented with chemicals (Figure 1A). Cells gradually migrated from colonies and proliferated during the induction (Figure 1B). Cells were harvested after 7 days of being induced, and were subsequently sorted according to the expression of p75 (Figure 1C). We detected two peaks in p75-positive populations, designated $p75^{low}$ and $p75^{high}$, and the efficiency of hNCC induction was evaluated based on the fraction of $p75^{high}$ cells.

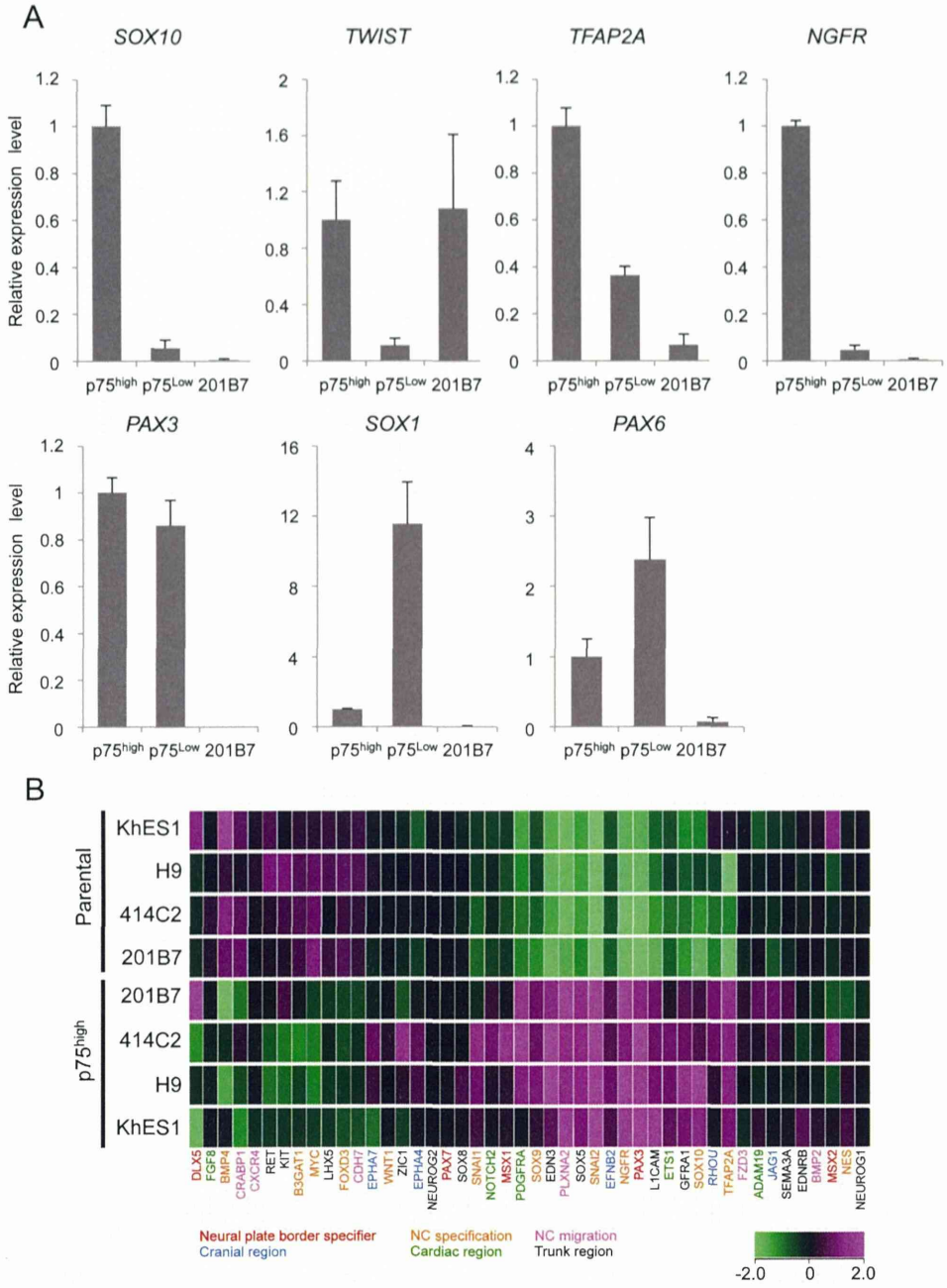

Figure 2. Expression profiles of sorted p75^{high} cells. A) The expression of marker genes in sorted p75^{high} and p75^{low} cells. The mRNA expression of each gene was analyzed by RT-qPCR in undifferentiated 201B7 (hiPSCs) and sorted p75^{low} and p75^{high} cells, and was shown as a relative value using the level in sorted p75^{high} cells as 1.0. Average ± SD. N=3, biological triplicates. B) Clustering analyses of NCC markers in p75^{high} populations from several hESC and hiPSC lines. Marker genes for each sub-population of NCCs were labeled using the indicated colors.

doi:10.1371/journal.pone.0112291.g002

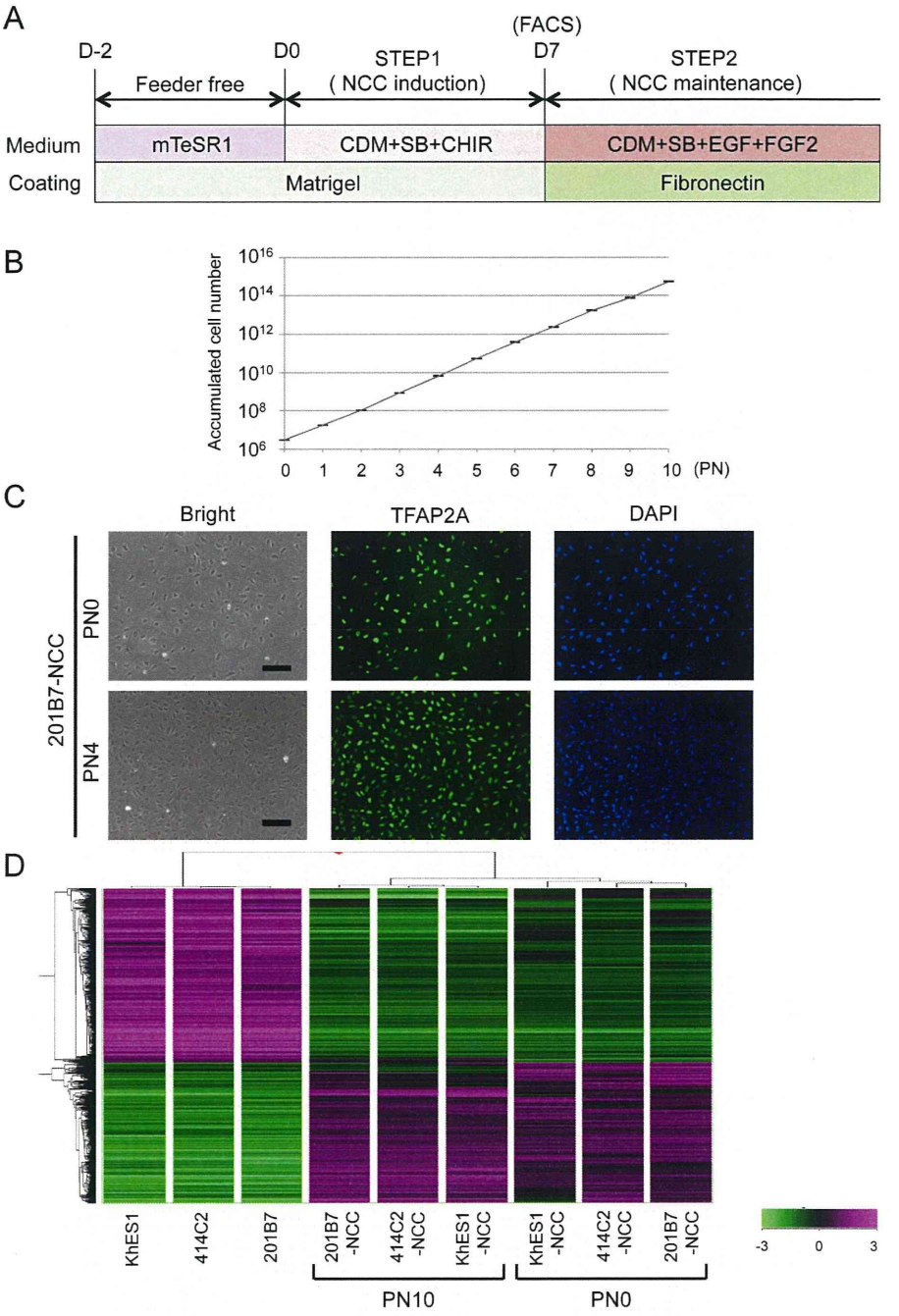

Figure 3. Sustained expansion of hNCCs with original characteristics. A) Schematic representation of the culture conditions. B) Growth profile of 201B7-derived hNCCs. Average ± SD. N=3, biological triplicate. C) Phase contrast images and immunostaining of TFAP2A in 201B7-derived hNCCs at PN0 and PN4, Scale bar, 200 μm. D) Hierarchical clustering analyses of hPSCs and hPSC-derived hNCCs at PN0 and PN10.

doi:10.1371/journal.pone.0112291.g003

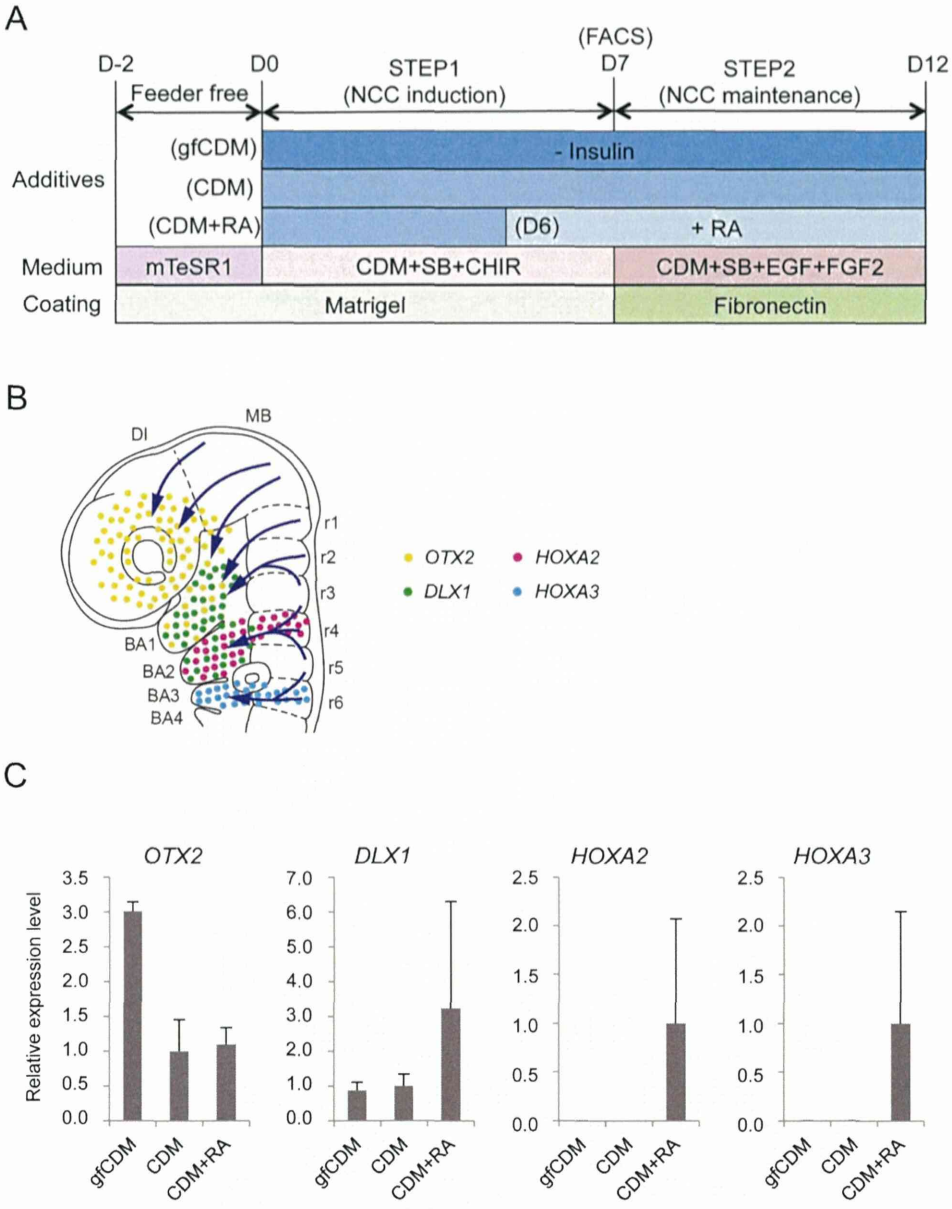

Figure 4. Modulation of regional characteristics of hNCCs. A) Schematic representation of culture conditions for the induction and maintenance of hNCCs. RA, retinoic acid (100 nM). B) Schematic distribution of marker-positive cells in the murine embryo. DI, diencephalon; MB, midbrain; BA1 to BA4, branchial arch 1 to branchial arch 4; r1 to r6; rhombomere 1 to rhombomere 6. C) The mRNA expression of regional specifier genes in hNCCs. $p75^{high}$ cells were collected at the end of the hNCC induction by FACS and seeded onto fibronectin-coated dishes. RNAs were extracted when cells reached a semi-confluent state and used for RT-qPCR. The relative expression level of each gene was demonstrated using the value of cells cultured in CDM (*OTX2* and *DLX1*) or CDM + RA (*HOXA2* and *HOXA3*) as 1.0. Average ± SD. N=3, biological triplicate.

doi:10.1371/journal.pone.0112291.g004

The effects of SB, which has been shown to inhibit Activin/Nodal/TGFβ signaling and induce neural cells and hNCCs from hPSCs without the help of other chemicals, were firstly evaluated [14]. In accordance with the reported data,

CDM supplemented with SB successfully delivered $p75^{high}$ cells with a PAX6-positive neuroectoderm from 201B7 (date not shown), while the induction efficiency of $p75^{high}$ cells was approximately 35% (0 μM in Figure 1C). The activation of Wnt signaling was previously shown to play a key role in the induction of hNCCs [14, 15], and can be achieved using the GSK3β inhibitor BIO or CHIR. Therefore, we attempted to determine the most effective concentration of CHIR with a fixed concentration of SB (10 μM) to induce $p75^{high}$ cells. The results obtained revealed that CHIR successfully induced $p75^{high}$ cells in a dose-dependent manner up to 1 μM, whereas higher concentrations of CHIR markedly inhibited the production of $p75^{high}$ cells (Figure 1C). We finally examined the effects of BMP signaling on this induction. The addition of BMP4 markedly inhibited the production of $p75^{high}$ cells, and these results were compatible with BMP signal inhibiting neural differentiation (Figure S1A). However, the treatment with DMH1 (10 μM), a specific inhibitor of SMAD1/5/8 phosphorylation, also reduced the $p75^{high}$ fraction (Figure S1B). The inhibitory effect of DMH1 on the induction of p75 was confirmed at different dosages, and other cytoplasmic (LDN193189) or extracellular (Noggin) inhibitors for BMP signaling also decreased the efficiency (Figure S1C). Therefore, the combination of SB (10 μM) and CHIR (1 μM) most effectively induced $p75^{high}$ cells from 201B7 hiPSCs. This result was reproduced in other hPSCs such as hESCs (H9, KhES1, and KhES3) and episomal hiPSCs (414C2) (Figure 1D). Most cells outgrowing from colonies were stained with NCC markers, p75 and TFAP2A, whereas the cells in colonies were positive for PAX6, a marker for the neuroectoderm (Figure 1E).

$p75^{high}$ cells expressed early NCC markers

The expression of marker genes were compared between $p75^{high}$ and $p75^{low}$ cells (Figure 2A). Sorted $p75^{high}$ cells expressed a number of genes in the early stage of NCCs, such as *SOX10*, *TWIST*, and *TFAP2A* genes. In contrast, the expression of these genes was significantly lower in the $p75^{low}$ fraction than in $p75^{high}$ fraction. The expression of *PAX3*, which is a marker both for NCCs and neurons, was high in both the $p75^{high}$ and $p75^{low}$ fractions. The expression of *PAX6* and *SOX1*, which are neural markers, was higher in the $p75^{low}$ fraction, which is consistent with some populations of p75-negative or TFAP2A-negative cells expressing *PAX6* (Figure 1E). These results indicated the relative enrichment of NCC cells in the $p75^{high}$ cell population.

In an attempt to further characterize $p75^{high}$ cells, genome-wide expression profiles were compared between sorted $p75^{high}$ cells and their corresponding hPSCs using a cDNA microarray (Affymetrix Gene 1.0 ST), and we found that the overall profiles of $p75^{high}$ cells derived from several PSCs were similar to each other (Figure S2). Based on the previous report [32], 46 genes were selected as markers for distinct NC-subpopulations and the expression level of these genes were compared between hNCCs and parental PSCs (Figure 2B). hNCCs in this study highly expressed early stage-related genes such as neural plate border specifier (PAX3) and NC specification (SNAI2, NGFR, TFAP2A, SOX9, and

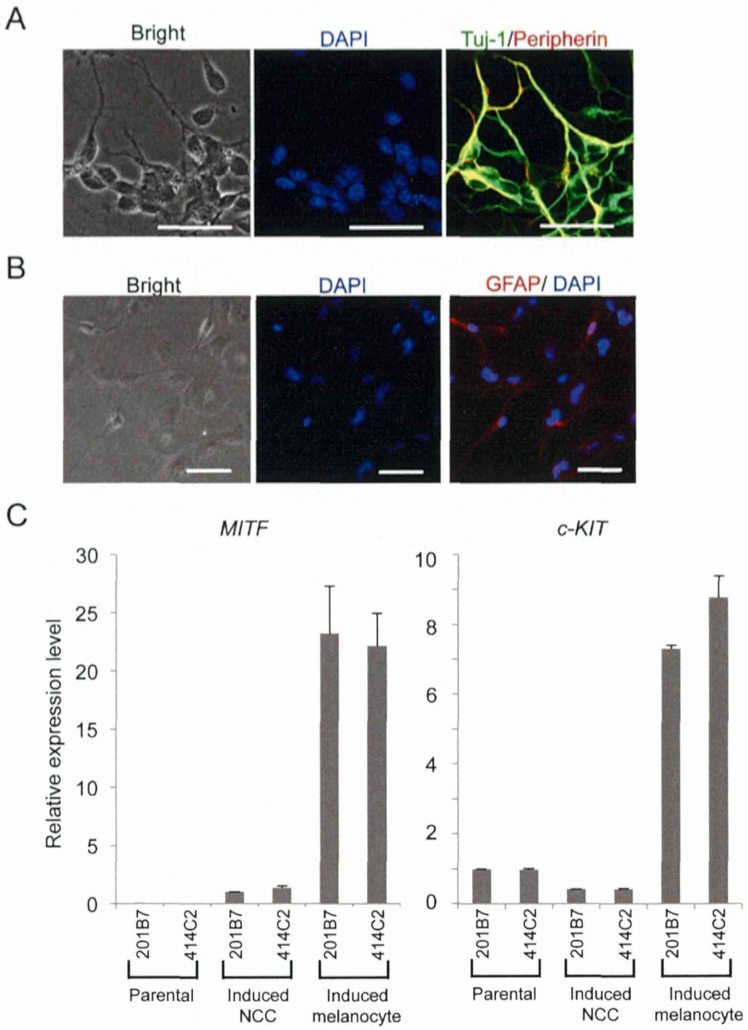

Figure 5. Derivation of peripheral neural cells, glia, and melanocytes from hNCCs. A) Neuronal differentiation of 201B7-derived hNCCs. Cells were stained with an antibody against peripherin (red) and Tuj-1 (green). B) The glial differentiation of 201B7-derived hNCCs. Cells were stained with an antibody against GFAP. Scale bar, 50 μm. C) Melanocyte differentiation of 201B7-derived hNCCs. The mRNA expression levels of *MITF* and *c-KIT* genes were shown as a relative value using the value in 201B7-derived hNCCs and 201B7 as 1.0, respectively. Average ± SD. N=3, biological triplicates.

doi:10.1371/journal.pone.0112291.g005

SOX10), but also some region-specifying genes (EFNB2 for cranial, PDGFRA for cardiac, and SOX5 for trunk region), suggesting the heterogeneous population of $p75^{high}$ cells, which were designated hNCCs hereafter. The profiles of the current hNCCs were compared with those of two PSC-derived NCCs, which were induced by different protocols in previous studies [15, 32] (Figure S3). Although the three types of PSC-derived NCCs all highly expressed some genes, such as SNAI2, their